

Unearthing the electroweak structure of warped 5D models

Abhishek M. Iyer¹ and K. Sridhar²

¹*INFN-Sezione di Napoli, Via Cintia, 80126 Napoli, Italia*

²*Department of Theoretical Physics, Tata Institute of Fundamental Research, Homi Bhabha Road, Colaba, Mumbai 400 005, India*

Heavy charged bosons, with masses in the range of a few TeV, are a characteristic of warped extra-dimensional models with bulk gauge fields. Rendering the latter consistent with electroweak precision tests typically requires either a deformation of the metric or extension of the gauge symmetry. We make here the first attempt at finding empirical discriminants which would tell these models apart. Demonstrating the power of simple kinematic observables involving same-sign leptons, we construct simple yet powerful statistical discriminants.

The Randall-Sundrum (RS) Model, as written down originally, invokes an extra space dimension y compactified on an S^1/Z^2 orbifold of radius R [1]. Two branes (UV and IR respectively) are located at the orbifold fixed points (end-points) $y = 0$ and $y = \pi R \equiv L$. The bulk has a strong AdS curvature, with its magnitude k only somewhat smaller than the Planck scale M_{Pl} . The solutions to the vacuum Einstein equations admit a static background with Lorentz invariance built in, namely the warped metric

$$ds^2 = e^{-2A(y)} \eta_{\mu\nu} dx^\mu dx^\nu - dy^2, \quad A(y) = \pm k|y|. \quad (1)$$

The gauge-hierarchy problem is resolved by choosing $kR \sim 12$ and with an IR localized Higgs, and electroweak scale at around 250 GeV materialises naturally on account of the warping.

However, the warping also affects all IR-localised fields and, in particular, mass scales which suppress dangerous higher-dimensional operators responsible for proton decay or neutrino masses are also lowered. This spells a disaster for the model. A way out is to consider only the Higgs to be localised on or near the IR brane [2–4]. Collectively known as Bulk RS models, these viable variations yield a bonus: localising fermions at different positions in the bulk implies differing overlaps of their profiles with the Higgs field. This then provides a natural mechanism for explaining fermion mass and mixing hierarchy and in addition, suppresses dangerous flavour-changing neutral currents (FCNCs). For reviews of bulk models, see Refs. [5] and [6].

Electroweak precision tests impose very strong constraints on bulk models. If, for example, only the gauge bosons propagate in the bulk, then the couplings of their KK modes to the IR-localised fermions lead to unacceptably large contributions to T and S , thereby resulting in a lower bound of about 25 TeV on the mass of the first KK mode of the gauge boson. A six-dimensional generalization of the RS model brings this mass limit down to about 7-8 TeV [7–9], but it is possible to stick to the original five-dimensional model and make other modifications to address the electroweak constraints. Localising the light fermions close to the UV brane, significantly reduces the

constraints from the S -parameter. The corrections to the T parameter can be softened by enlarging the gauge symmetry in the bulk to $SU(3)_c \times SU(2)_L \times SU(2)_R \times U(1)_y$ [10, 11] Appropriate choice of the fermion representations also helps suppress contributions in the non-oblique $Z \rightarrow b\bar{b}$ corrections [12, 13].

An alternative to enhanced gauge symmetry is to use a deformed metric near the IR brane [14, 15], with the softening of the singularity at the IR boundary implying that the Higgs is a bulk scalar field. The function $A(y)$ in Eq. 1 is now modified to

$$A(y) = ky - \nu^{-2} \log(1 - y/y_s) \quad (2)$$

(the limit $\nu \rightarrow 0$ reverting to the RS geometry). The UV brane is still located at $y = 0$. The IR brane is, however, located at $y = y_1$ with the position of the singularity ($y = y_s$) located behind it at $y_s \simeq y_1 + \mathcal{O}(k^{-1})$. To address the hierarchy one requires $A(y_1) \sim 35$, which fixes the value of y_1 . The deformation causes the Higgs field to be moved further away from the IR brane whereas the gauge boson KK modes move towards it. The consequent reduction in the overlap of the Higgs and KK gauge boson modes reduces the bounds from the T parameter and the mass of first KK gauge boson mode can now be as small as 1.5 TeV [13].

In typical Bulk RS models, the gauge boson KK excitations are the lightest ones. Constituting the most promising probes, searches of KK excitations of gluons [16–20], electroweak gauge bosons [21, 22] and the Higgs [23, 24] have been proposed and some of these executed by the ATLAS [25] and CMS experiments [26].

We are interested in distinguishing between the deformed and the custodial model at the LHC. In the custodial model, the SM fermion doublets are extended to fields transforming as $(2, 2)$. The quark multiplet thus contains exotic $\chi_{5/3}$ fermions absent in the deformed model. We look at the production of these states, in association with a top, from the decay of the first KK-mode of the W^\pm bosons. Cascade decays of the $\chi_{5/3}$ fermion leads to two leptons with the same sign. Such final states are also possible in deformed scenarios, where a heavy gauge boson decays in to a vector-like-quark and

a top. However, the two cases are characterized by different kinematics and we demonstrate that simple kinematic variables like the azimuthal separation $\Delta\phi$ between the same sign leptons and p_T combinations of the same sign leptons are effective in not only suppressing the background but also in distinguishing between the two scenarios.

The third generation quarks being localized close to the IR brane, the coupling of a KK- W'^+ to a $t\bar{b}$ pair is quite similar to that to a VLQ-SM quark pair. Thus, owing to the larger phase space available, the KK- W'^+ would decay primarily into the former channel, rendering this the discovery mode. Several dedicated analyses in this direction have used combinations of different variables (both kinematic and substructure) to extract the maximum signal efficiency. Instead, we perform a minimal LHC analysis to set up the discovery mode and demonstrate a simple set of cuts to achieve a $\sim 3\sigma$ sensitivity for the process $p p \rightarrow W'^+ \rightarrow t\bar{b}$. The matrix element for this process is generated using MADGRAPH 6 [27] using the model files generated by FEYNRULES. To maximize discovery potential hadronic decay of the top is considered. Generated events are passed on to PYTHIA 8 [28] for showering and hadronization. For $m_{W'} \sim 2.5$ TeV, the decay partons are likely to be associated with very high transverse momentum (p_T) jets. The jet reconstruction radius must be such that the decay products of the top are captured within a cone of radius R , with the opening angle roughly being $\sim 2m_t/p_T^t$, where p_T^t is the top transverse momentum. It is clear that a radius $R = 0.5$ is sufficient for the kinematics under consideration. Using FASTJET, [29] with the Cambridge-Aachen [30] jet clustering algorithm and require that the jets satisfy $p_T > 100$ GeV. The top candidate is identified among the two leading jets, using the HEP TOP TAGGER [31] algorithm.

Post top-identification, we demand that the invariant mass of the two jet system satisfies $2000 < m_{j_0j_1} < 3000$ GeV. To estimate the background, we simulate hard QCD processes in the following kinematic regime: require the scalar sum of the visible transverse momenta to be $\sum p_T^j > 500$ GeV and the invariant mass of the outgoing partons to be $\hat{m}_{\text{jets}} > 800$ GeV. Taking into account the width of the resonance as well as the mass resolution of the final states, the background is generated with these choices of parameters. These values are chosen as the decay constituents of W' are likely to have a p_T of at least 500-600 GeV each. This reduces the QCD cross-section to 10^5 fb. Furthermore, after the selection criteria detailed above are imposed, the QCD background has a fake rate of 0.1% while the signal has an acceptance of 13%. Given the current bounds from LHC, the production cross-section for the W' is chosen to be 20 fb.¹ This

leads to a rough sensitivity of $S/\sqrt{B} \sim 3$ with ~ 400 fb^{-1} of data. It is to be stressed that this acceptance can be significantly improved with even lesser luminosity. However, it has been considered extensively and is not the goal of this paper. The objective behind this section was to demonstrate that even the most basic cuts is sufficient to obtain a reasonable signal acceptance. Post this discovery, it is then necessary to extract the origin of the heavy charged object: whether the origin of the heavy gauge state is due to a SM gauge symmetry or due to an extended gauge group. One simple way is to look at the charge of the heavy fermion the W' decays into, as determined by analysing the multileptonic final state.

For custodial models, the electroweak gauge group is extended to $SU(2)_L \times SU(2)_R \times U(1)_{B-L}$. The (t, b) doublet is replaced by a bidoublet represented by $Q_3 \equiv \begin{bmatrix} \chi_{5/3} & t \\ T_{2/3} & b \end{bmatrix}$ where χ, T are exotic fermions with electromagnetic charges 5/3, 2/3 respectively. The crucial difference between the deformed and the custodial models is the presence of the charge 5/3 state. For simplicity we consider t_R to be a gauge singlet. and consider the decay of the $W^{(1)}$ is into $\chi_{5/3}\bar{t}$. The $\chi_{5/3}$ can further decay into Wt resulting in a $Wt\bar{t}$ final state. Considering a total leptonic final state, this leads to three leptons with two leptons of the same sign.

For deformed models, the gauge structure is SM like and hence the heavy KK fermions also have charges $Q = 2/3, -1/3$. The aforementioned three lepton final state can arise in two ways: A) The VLQ decays into a tZ or bZ as the case may be. Thus, the net final state from the gauge KK state is $t\bar{b}Z$. Assuming both the top and the Z decay leptonically, we have a 3 lepton final state. with 2 leptons of same sign. This case can however be distinguished using a Z mass veto for two leptons with opposite sign.

B) If the KK fermion decays into $W\bar{b}$ ($Q = 2/3$) and W^-t ($Q = -1/3$), the overall final state from the gauge-KK would be $W\bar{b}b$ and $W\bar{t}t$ respectively. The former leads to only a single isolated hard lepton, while the latter may lead to three leptons and two b-tagged jets.

Variables for discrimination:

In order to distinguish the two scenarios, it is necessary to understand the kinematic features for the two gauge structures. Since the signal is characterized by the presence of two leptons of the same sign, it is useful to construct variables using these two leptons:

$\Delta\phi_{l\pm l\pm}$ between the same-sign leptons: For the custodial case, the two same sign leptons originate from the decay of the 5/3 state. As a result the $\Delta\phi$ between them would depend on the boost of the VLQ. For the deformed case, on the other hand, one of them is due

¹ This is the typical value for the production cross-section for charged bosons in extra-dimensional models.

to the decay of the VLQ while the other is due to the top originating from the heavy charged vector boson. Since the VLQ and the top from the charged boson are produced back-to-back, the same-sign leptons from them are also broadly separated. As a result the utility of this variable to segregate the two cases depends on the benchmark point used. We consider the following four different combinations of bench mark points:

$$\begin{aligned} \text{BP1} &:: (3000, 1500) & \text{BP2} &:: (3000, 1000) \\ \text{BP3} &:: (3500, 1500) & \text{BP4} &:: (3500, 2000) \end{aligned} \quad (3)$$

where the masses are expressed as $(m_{W'}, m_{VLQ})$. For the background the same sign lepton is due to radiation off one of the tops and hence has a very distinct distributions where the $\Delta\phi_{l\pm l\pm}$ are either back-to-back or in the same direction. This is extremely useful in distinguishing the background from the signal. Fig. 1 gives the distribution of this variables for the different benchmark points and the background. The deformed models are characterized by a fairly similar distribution for all the benchmark points. It can be seen that the efficiency of this variable is better for BP2 over others and can be attributed to the larger boost of 1 TeV VLQ states from the decay of W' .

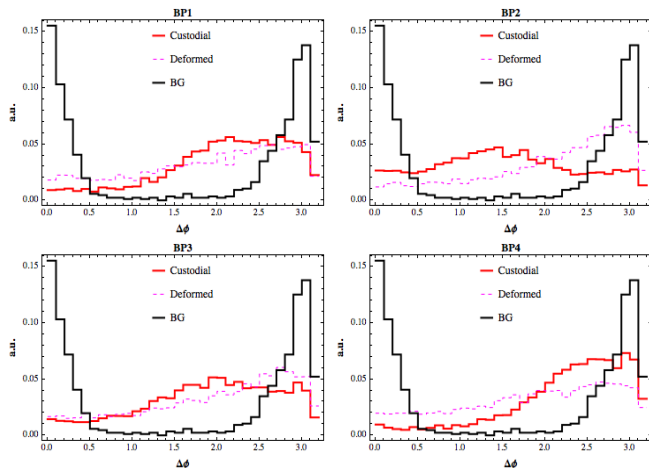


FIG. 1. $\Delta\phi$ between the same sign leptons for the 4 benchmark points.

p_T^{min} of the same sign-lepton combination ($p_T^{min} = \min(p_T^{l_1^\pm}, p_T^{l_2^\pm})$). For the deformed models one of the same sign leptons is due to the SM W originating from the decay of the VLQ while the other is due to the top from the heavy gauge boson vertex. Due to the boost of the top, the corresponding lepton from this top is characterized by larger p_T than the one due to the W from the decay of the VLQ. Left plot of Fig. 2 gives the comparison of parton level p_T for the W and the top

from the VLQ. While the W is characterized by smaller transverse momentum, it is only shared between lepton and the neutrino. Resultantly, the p_T^{min} of the same sign lepton combination is likely to have a momentum distribution peaking at relatively larger values as shown by the dashed-pink line at the bottom plot of Fig. 2.

For custodial models on the other hand, the two same-sign leptons are from the decay products of the VLQ. The right plot of Fig. 2 gives a comparison of the p_T for W and the top from $\chi_{5/3}$ VLQ. Since the p_T is shared between three objects: b -jet, lepton and neutrino, the corresponding lepton is characterized by relatively lower p_T than in the case when the decay proceeds due a non-custodial scenario. This is evident by the distribution of the solid red line in the bottom plot in Fig. 2.

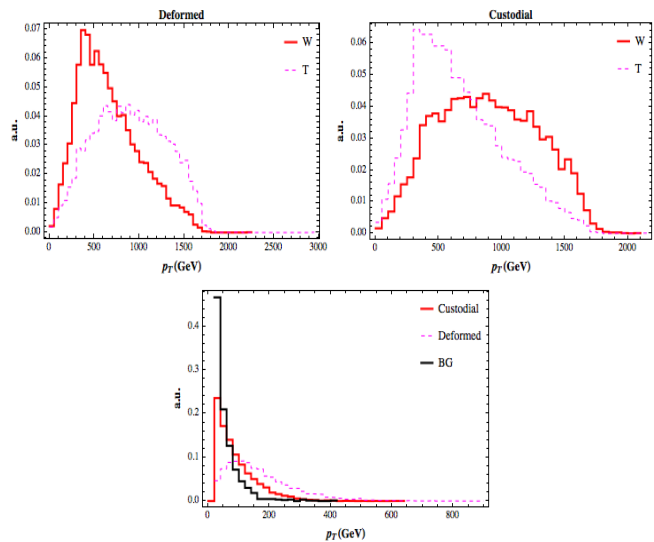


FIG. 2. Plots in the top row give the parton p_T of the decay products of the VLQ for deformed (left) and for custodial (right) scenarios. The bottom plot gives the distribution of the minimum transverse momentum between the same sign lepton combination $p_T^{min} = \min(p_T^{l_1^\pm}, p_T^{l_2^\pm})$

Given the two distributions, it is necessary to develop a quantitative measure to distinguish them. We assume that one particular Hypothesis say H_T , to be true, which is to be tested against the alternative hypothesis say H_A . To estimate the number of events N required to disfavour a given spin hypothesis H_A to some factor R , we solve

$$\frac{1}{R} = \frac{p(H_A|N \text{ events from } H_T)}{p(H_T|N \text{ events from } H_T)} \quad (4)$$

where R is integer and implies that the alternative hypothesis H_A is disfavoured at 1 : R odds in favour of H_T . Following [33, 34], we present results for $R = 20, 1000$. The N events are characterized by their values of either one or a set of observables \mathcal{O}_i . In the first instance we choose two possibilities: either $\mathcal{O}_1 = \Delta\phi$ or $\mathcal{O}_1 = p_T^{min}$

between the same-sign lepton candidates. We find that while the former is useful for background discrimination, the latter is more efficient for distinguishing the two models. Following, this we adapt an analysis involving both the variables simultaneously. Following the steps in [33] for the discrete implementation of Kullback-Leibler divergence [34], Eq. 4 becomes:

$$\log\left(\frac{1}{R}\right) = \sum_{i=1}^K \left[\mu_j^{(T)} \log \frac{\mu_j^{(A)}}{\mu_j^{(T)}} + \mu_j^{(T)} - \mu_j^{(A)} \right]. \quad (5)$$

where μ_j is the expectation value for the number of events in the j^{th} bin for a given hypothesis. To translate the above expression into the number of events (and hence the integrate luminosity \mathcal{L}) required to separate H_A from H_T at 1 : R we use

$$\mu_j^{(X)} = \mathcal{L} \sigma_{tot}^{(W')} \text{B.R.}(W' \rightarrow l^+ l^- l^+ + X) \epsilon_j^{(X)}, \quad (6)$$

where X denotes jets and missing energy and ϵ_j is the collider acceptance efficiency for the j^{th} bin. ²

Using Eq. 5 and Eq. 6 and $N_R = \mathcal{L} \sigma_{tot}$, the number of events N_R of the true hypothesis H_T to disfavour H_A at 1 : R odds is

$$N_R = \frac{\log R}{\sum_{j=1}^K \left[\epsilon_j^{(T)} \log \frac{\epsilon_j^{(A)}}{\epsilon_j^{(T)}} + \epsilon_j^{(A)} - \epsilon_j^{(T)} \right]}. \quad (7)$$

Results of the analysis: We employ this analysis for the different benchmark masses in Eq. 3. The typical model cross-section for 3 TeV state for deformed models is < 1 fb while that for custodial models ~ 15 fb for deep UV localization of the light quarks. One may argue that on account of the different cross-sections a relatively ‘early’ discovery is more likely to be a sign of custodial models over deformed models. However, direct searches in the di-jet (tb) final state may give a clear hint of the underlying resonance only if it has a sufficiently narrow width. In the event of a broad-width, the mass resolution is not likely to be as precise. For the purpose of comparison we assume a similar production cross-section for both scenarios. ³ Upper limits exist on $\sigma(pp \rightarrow W') \times \text{B.R.}(W' \rightarrow tb)$ from direct searches on the tb final state [35] where masses below 3 TeV with $\sigma(pp \rightarrow W') \times \text{B.R.}(W' \rightarrow tb) > 15$ fb are excluded. We assume a production cross section of 15 fb for 3 TeV and 5 fb for 3.5 TeV. Table I gives the results of the statistical discussion using using both $p_T^{\text{min}} - \Delta\phi_{l\pm l\pm}$. We

present results for both $R = 20$ (black) and $R = 1000$ (red). The probabilities are computed by constructing bins of sizes (0.7, 145) in the $\Delta\phi_{l\pm l\pm} - p_T^{\text{min}}$ over the range $[0 - \pi, 0 - 570]$. While p_T^{min} of the same sign lepton combination is extremely useful in distinguishing the two scenarios, it is not as effective as $\Delta\phi_{l\pm l\pm}$ for background discrimination. Note that the conclusions using both variables are expected to be similar within statistical fluctuations to those which takes only p_T^{min} into account. This is because p_T^{min} plays the dominant role for the discrimination in both cases while $\Delta\phi_{l\pm l\pm}$ is practically a dummy variable as far as the discrimination between the two signal possibilities are concerned. We reiterate that the role $\Delta\phi_{l\pm l\pm}$ is primarily restricted to segregating both the signal possibilities from the background. Given the drastically different distributions of $\Delta\phi_{l\pm l\pm}$ for the background from the signal possibilities 3-4 events are suffice to eliminate the background only hypothesis at a 1 : 20 odds.

BP1			BP2		
N_R	Custodial	Deformed	N_R	Custodial	Deformed
Custodial	∞	16 39	Custodial	∞	13 30
Deformed	11 27	∞	Deformed	6 15	∞
BP3			BP4		
N_R	Custodial	Deformed	N_R	Custodial	Deformed
Custodial	∞	20 47	Custodial	∞	14 34
Deformed	12 29	∞	Deformed	9 22	∞

TABLE I. Table gives the expected number of events $N_R = \mathcal{L} \sigma_{tot}^{(X)}$, to disfavour the column hypothesis (H_A) in favour of the row hypothesis (H_T) by a factor of $R = 20$ (black) and $R = 1000$ (red) at the 13 TeV LHC. Both p_T^{min} and $\Delta\phi_{l\pm l\pm}$ variables are used in this case.

Discussions: The results in Table I can be converted to the required luminosity by simply assuming a production cross-section for the W' and the branching fraction for the VLQ into the corresponding states. For simplicity we discuss the results for $R = 20$ and assume equal production cross-sections and branching fractions for both the models. If we assume a production cross-section of 15 fb, with an integrated luminosity of 3000 fb⁻¹, branching fractions as low as 20% for the VLQ T ⁴ can be probed. The results of Table I are very general and can be used to discriminate other classes of models with a similar gauge and fermion content.

Heavy charged gauge bosons are a characteristic feature of several extensions beyond the Standard Model.

² We assume that $\sigma_{tot}^{(W')}$ is same for both the hypothesis $X = A, T$.

³ The production cross-sections for the deformed case can be enhanced by slightly enhancing the couplings of the light quarks to the KK gauge fields while respecting a $U(2)$ symmetry in the coupling space.

⁴ We assume $\text{B.R.}(W' \rightarrow TX) \sim 50\%$, where X is SM state.

Corresponding to the gauge origins of these heavy vectors, the representation of the fermion content also differ. Using this as a motivation, we present a methodology to distinguish the two cases in the event of a discovery. We demonstrate effectiveness of this technique by using a statistical tool which utilizes simple kinematic variables like $\Delta\phi$ between the same-sign leptons and p_T . Given the generic nature of the method, the analysis and the corresponding results can also be extended with similar gauge and fermion content.

ACKNOWLEDGMENTS

We are grateful to Debajyoti Choudhury for several useful discussions and a careful reading of the manuscript. A.I. was supported in part by MIUR under Project No. 2015P5SBHT and by the INFN research initiative ENP. K.S. work is partly supported by a project grant from the Indo-French Centre for the Promotion of Advanced Research (project no. 5904-2).

-
- [1] L. Randall and R. Sundrum, Phys.Rev.Lett. **83**, 3370 (1999), arXiv:hep-ph/9905221 [hep-ph].
- [2] A. Pomarol, Phys.Lett. **B486**, 153 (2000), arXiv:hep-ph/9911294 [hep-ph].
- [3] T. Gherghetta and A. Pomarol, Nucl.Phys. **B586**, 141 (2000), arXiv:hep-ph/0003129 [hep-ph].
- [4] Y. Grossman and M. Neubert, Phys.Lett. **B474**, 361 (2000), arXiv:hep-ph/9912408 [hep-ph].
- [5] T. Gherghetta, Physics of the Large and the Small, Proceedings of the Theoretical Advanced Study Institute in Elementary Particle Physics, - TASI 2009 (eds. C. Csaki and S. Dodelson) (2010), arXiv:1008.2570 [hep-ph].
- [6] S. Raychaudhuri and K. Sridhar, *Particle Physics of Brane Worlds and Extra Dimensions*, 1419790 (Cambridge University Press, 2016).
- [7] M. T. Arun and D. Choudhury, JHEP **09**, 202 (2015), arXiv:1501.06118 [hep-th].
- [8] M. T. Arun and D. Choudhury, JHEP **04**, 133 (2016), arXiv:1601.02321 [hep-ph].
- [9] M. T. Arun and D. Choudhury, Nucl. Phys. **B923**, 258 (2017), arXiv:1606.00642 [hep-th].
- [10] K. Agashe, A. Delgado, M. J. May, and R. Sundrum, JHEP **0308**, 050 (2003), arXiv:hep-ph/0308036 [hep-ph].
- [11] K. Agashe, R. Contino, L. Da Rold, and A. Pomarol, Phys.Lett. **B641**, 62 (2006), arXiv:hep-ph/0605341 [hep-ph].
- [12] H. Davoudiasl, S. Gopalakrishna, E. Ponton, and J. Santiago, New J. Phys. **12**, 075011 (2010), arXiv:0908.1968 [hep-ph].
- [13] A. M. Iyer, K. Sridhar, and S. K. Vempati, Phys. Rev. **D93**, 075008 (2016), arXiv:1502.06206 [hep-ph].
- [14] J. A. Cabrer, G. von Gersdorff, and M. Quiros, Phys.Lett. **B697**, 208 (2011), arXiv:1011.2205 [hep-ph].
- [15] J. A. Cabrer, G. von Gersdorff, and M. Quiros, JHEP **05**, 083 (2011), arXiv:1103.1388 [hep-ph].
- [16] K. Agashe, A. Belyaev, T. Krupovnickas, G. Perez, and J. Virzi, Phys.Rev. **D77**, 015003 (2008), arXiv:hep-ph/0612015 [hep-ph].
- [17] B. Lillie, L. Randall, and L.-T. Wang, JHEP **0709**, 074 (2007), arXiv:hep-ph/0701166 [hep-ph].
- [18] M. Guchait, F. Mahmoudi, and K. Sridhar, Phys.Lett. **B666**, 347 (2008), arXiv:0710.2234 [hep-ph].
- [19] B. C. Allanach, F. Mahmoudi, J. P. Skittrall, and K. Sridhar, JHEP **1003**, 014 (2010), arXiv:0910.1350 [hep-ph].
- [20] A. M. Iyer, F. Mahmoudi, N. Manglani, and K. Sridhar, Phys. Lett. **B759**, 342 (2016), arXiv:1601.02033 [hep-ph].
- [21] K. Agashe, S. Gopalakrishna, T. Han, G.-Y. Huang, and A. Soni, Phys. Rev. **D80**, 075007 (2009), arXiv:0810.1497 [hep-ph].
- [22] K. Agashe, H. Davoudiasl, S. Gopalakrishna, T. Han, G.-Y. Huang, G. Perez, Z.-G. Si, and A. Soni, Phys. Rev. **D76**, 115015 (2007), arXiv:0709.0007 [hep-ph].
- [23] F. Mahmoudi, U. Maitra, N. Manglani, and K. Sridhar, JHEP **11**, 075 (2016), arXiv:1608.07407 [hep-ph].
- [24] F. Mahmoudi, N. Manglani, and K. Sridhar, (2017), arXiv:1712.04966 [hep-ph].
- [25] G. Aad *et al.* (ATLAS), JHEP **08**, 148 (2015), arXiv:1505.07018 [hep-ex].
- [26] S. Chatrchyan *et al.* (CMS), JHEP **09**, 029 (2012), [Erratum: JHEP03,132(2014)], arXiv:1204.2488 [hep-ex].
- [27] J. Alwall, R. Frederix, S. Frixione, V. Hirschi, F. Maltoni, O. Mattelaer, H. S. Shao, T. Stelzer, P. Torrielli, and M. Zaro, JHEP **07**, 079 (2014), arXiv:1405.0301 [hep-ph].
- [28] T. Sjostrand, S. Ask, J. R. Christiansen, R. Corke, N. Desai, P. Ilten, S. Mrenna, S. Prestel, C. O. Rasmussen, and P. Z. Skands, Comput. Phys. Commun. **191**, 159 (2015), arXiv:1410.3012 [hep-ph].
- [29] M. Cacciari, G. P. Salam, and G. Soyez, Eur. Phys. J. **C72**, 1896 (2012), arXiv:1111.6097 [hep-ph].
- [30] Y. L. Dokshitzer, G. D. Leder, S. Moretti, and B. R. Webber, JHEP **08**, 001 (1997), arXiv:hep-ph/9707323 [hep-ph].
- [31] T. Plehn, M. Spannowsky, M. Takeuchi, and D. Zerwas, JHEP **10**, 078 (2010), arXiv:1006.2833 [hep-ph].
- [32] J. M. Smillie and B. R. Webber, JHEP **10**, 069 (2005), arXiv:hep-ph/0507170 [hep-ph].
- [33] B. C. Allanach, D. Bhatia, and A. M. Iyer, Eur. Phys. J. **C77**, 595 (2017), arXiv:1706.09039 [hep-ph].
- [34] C. Athanasiou, C. G. Lester, J. M. Smillie, and B. R. Webber, JHEP **08**, 055 (2006), arXiv:hep-ph/0605286 [hep-ph].
- [35] M. Aaboud *et al.* (ATLAS), Phys. Lett. **B781**, 327 (2018), arXiv:1801.07893 [hep-ex].